





Article

Effective Modulation by Lacosamide on Cumulative Inhibition of I_{Na} during High-Frequency Stimulation and Recovery of I_{Na} Block during Conditioning Pulse Train

Po-Ming Wu ^{1,2,†}, Yu-Ching Lin ^{3,†}, Chi-Wu Chiang ⁴, Hsin-Yen Cho ⁵, Tzu-Hsien Chuang ⁵, Meng-Cheng Yu ⁵, Sheng-Nan Wu ^{5,6,*}  and Yi-Fang Tu ^{1,2,*} 

¹ Institute of Clinical Medicine, College of Medicine, National Cheng Kung University, Tainan 70101, Taiwan

² Department of Pediatrics, National Cheng Kung University Hospital, College of Medicine, National Cheng Kung University, Tainan 70101, Taiwan

³ Department of Physical Medicine and Rehabilitation, National Cheng Kung University Hospital, College of Medicine, National Cheng Kung University, Tainan 70101, Taiwan

⁴ Institute of Molecular Medicine, College of Medicine, National Cheng Kung University, Tainan 70101, Taiwan

⁵ Department of Physiology, College of Medicine, National Cheng Kung University, Tainan 70101, Taiwan

⁶ Institute of Basic Medical Sciences, College of Medicine, National Cheng Kung University, Tainan 70101, Taiwan

* Correspondence: snwu@mail.ncku.edu.tw (S.-N.W.); nckutu@gmail.com (Y.-F.T.);

Tel.: +886-6-2353535-5334 (S.-N.W.); +886-6-2353535-5273 (Y.-F.T.); Fax: +886-6-2362780 (S.-N.W.)

† Co-First Author: These authors contributed equally to this work.



Citation: Wu, P.-M.; Lin, Y.-C.; Chiang, C.-W.; Cho, H.-Y.; Chuang, T.-H.; Yu, M.-C.; Wu, S.-N.; Tu, Y.-F. Effective Modulation by Lacosamide on Cumulative Inhibition of I_{Na} during High-Frequency Stimulation and Recovery of I_{Na} Block during Conditioning Pulse Train. *Int. J. Mol. Sci.* **2022**, *23*, 11966. <https://doi.org/10.3390/ijms231911966>

Academic Editor: Asim Debnath

Received: 12 September 2022

Accepted: 4 October 2022

Published: 8 October 2022

Publisher's Note: MDPI stays neutral with regard to jurisdictional claims in published maps and institutional affiliations.



Copyright: © 2022 by the authors. Licensee MDPI, Basel, Switzerland. This article is an open access article distributed under the terms and conditions of the Creative Commons Attribution (CC BY) license (<https://creativecommons.org/licenses/by/4.0/>).

Abstract: The effects of lacosamide (LCS, Vimpat[®]), an anti-convulsant and analgesic, on voltage-gated Na^+ current (I_{Na}) were investigated. LCS suppressed both the peak (transient, $I_{Na(T)}$) and sustained (late, $I_{Na(L)}$) components of I_{Na} with the IC_{50} values of 78 and 34 μM found in GH₃ cells and of 112 and 26 μM in Neuro-2a cells, respectively. In GH₃ cells, the voltage-dependent hysteresis of persistent I_{Na} ($I_{Na(P)}$) during the triangular ramp pulse was strikingly attenuated, and the decaying time constant (τ) of $I_{Na(T)}$ or $I_{Na(L)}$ during a train of depolarizing pulses was further shortened by LCS. The recovery time course from the I_{Na} block elicited by the preceding conditioning train can be fitted by two exponential processes, while the single exponential increase in current recovery without a conditioning train was adequately fitted. The fast and slow τ 's of recovery from the I_{Na} block by the same conditioning protocol arose in the presence of LCS. In Neuro-2a cells, the strength of the instantaneous window I_{Na} ($I_{Na(W)}$) during the rapid ramp pulse was reduced by LCS. This reduction could be reversed by tefluthrin. Moreover, LCS accelerated the inactivation time course of I_{Na} activated by pulse train stimulation, and veratridine reversed its decrease in the decaying τ value in current inactivation. The docking results predicted the capability of LCS binding to some amino-acid residues in sodium channels owing to the occurrence of hydrophobic contact. Overall, our findings unveiled that LCS can interact with the sodium channels to alter the magnitude, gating, voltage-dependent hysteresis behavior, and use dependence of I_{Na} in excitable cells.

Keywords: lacosamide (Vimpat[®]); voltage-gated Na^+ current; transient (peak) Na^+ current; late Na^+ current; persistent Na^+ current; window Na^+ current; hysteresis; cumulative inhibition; current recovery

1. Introduction

LCS, a functionalized amino acid, is an antiepileptic and analgesic drug available orally and intravenously in clinical practice [1–6]. It is commonly administrated in patients with epilepsy and occasionally in patients with trigeminal neuralgia or other neuropathic pain [1,5,7–12]. A growing body of evidence demonstrated the effectiveness and tolerability of LCS in patients with epilepsy [13–19]. Earlier reports have shown that this compound can decrease the frequency of interictal spikes as well as high-frequency oscillations in mesial temporal lobe epilepsy or refractory focal epilepsy [13,20]. The antiepileptic ability

of LCS was proposed mainly because it selectively enhances the voltage-dependence of the slow inactivation of Na^+ current (I_{Na}) [5,7,21–23]. In addition to its antiepileptic effects, additional broad effects of LCS have been observed clinically [3,4]. For instance, a recent report showed that LCS could alter electrocardiographic changes in a status epilepticus animal model [24]. Another report showed that LCS could induce personality changes, which disappeared after its discontinuation [25]. Additional electrophysiological actions of LCS might explain its multiple therapeutic effects and need to be thoroughly established.

The voltage-gated Na^+ currents form voltage-gated sodium channels (Na_v) are critical for the generation and propagation of action potentials in excitable membranes [26,27]. These channels can briefly shift from the resting to the open state after depolarization, thereby allowing the flow of Na^+ from the extracellular solution into the cell under the driving forces of the electrical and chemical gradients. After opening briefly in a voltage-dependent manner, the channels are shifted to the inactivated state(s), rendering I_{Na} intense but brief [27]. In addition to the voltage-dependence of the slow inactivation of I_{Na} , LCS has also been shown to enhance the frequency-dependent inhibition of I_{Na} [28]. However, whether the accumulative inhibition of I_{Na} inactivation during repetitive depolarization and/or recovery from I_{Na} inactivation during the preceding conditioning pulse train could be perturbed by LCS has not been adequately investigated. In the current study, the following attempts were undertaken to evaluate how LCS could lead to any adjustments to the magnitude, gating kinetics, voltage-dependent hysteresis ($\text{Hys}_{(V)}$), and use dependence of I_{Na} residing in two different excitable cells, pituitary tumor (GH₃) cells and neuroblastoma (Neuro-2a) cells. The observations could help to delineate the delicate modulation of functional activities in excitable cells occurring in vivo.

2. Results

2.1. Effects of LCS on Voltage-Gated Na^+ Current (I_{Na})

For the first stage of experiments, whether LCS would exert any perturbations on I_{Na} was tested. Pituitary tumor (GH₃) cells were placed in Ca^{2+} -free, Tyrode's solution, which contained 10 mM tetraethylammonium chloride (TEA) and 0.5 mM CdCl_2 to avoid interference by other types of ionic currents, such as K^+ and Ca^{2+} currents. Upon membrane depolarization from a holding potential of -100 mV to -10 mV for 30 milliseconds (msec), the transient I_{Na} ($I_{\text{Na(T)}}$) was elicited, and it could be attenuated dose-dependently by LCS (Figure 1A). At one minute after adding 30 μM or 100 μM LCS, the $I_{\text{Na(T)}}$ amplitude measured at the beginning of the depolarizing pulse was attenuated to 1012 ± 29 pA ($n = 8$, $p < 0.05$) or 783 ± 22 pA ($n = 8$, $p < 0.05$) from a control value of 1212 ± 32 pA ($n = 8$), respectively. When LCS was removed, the current amplitude returned to 1207 ± 31 pA ($n = 8$).

In addition, late I_{Na} ($I_{\text{Na(L)}}$) was measured at the end of the depolarizing test pulse. The extent of LCS-mediated inhibition of $I_{\text{Na(L)}}$ was higher than that at the start of the pulse (i.e., $I_{\text{Na(T)}}$). For example, 100 μM LCS decreased the $I_{\text{Na(L)}}$ amplitude from 74 ± 9 pA to 29 ± 9 pA ($n = 8$, $p < 0.05$). Meanwhile, upon exposure to 100 μM LCS, the slow component in the inactivation time constant (τ) of $I_{\text{Na(T)}}$ decreased from 12.2 ± 2.1 to 8.1 ± 1.3 msec ($n = 8$, $p < 0.05$). The relationship between LCS concentration and the inhibition of $I_{\text{Na(T)}}$ and $I_{\text{Na(L)}}$ is constructed in Figure 1B. It demonstrated a differential dose-dependent LCS-mediated inhibition in $I_{\text{Na(T)}}$ and $I_{\text{Na(L)}}$ elicited by the rapid membrane depolarization. Based on a modified Hill equation described in Materials and Methods, the IC_{50} values required for exerting a suppressive effect on $I_{\text{Na(T)}}$ and $I_{\text{Na(L)}}$ were further estimated as 78 and 34 μM , respectively, reflecting that these two values are distinguishable.

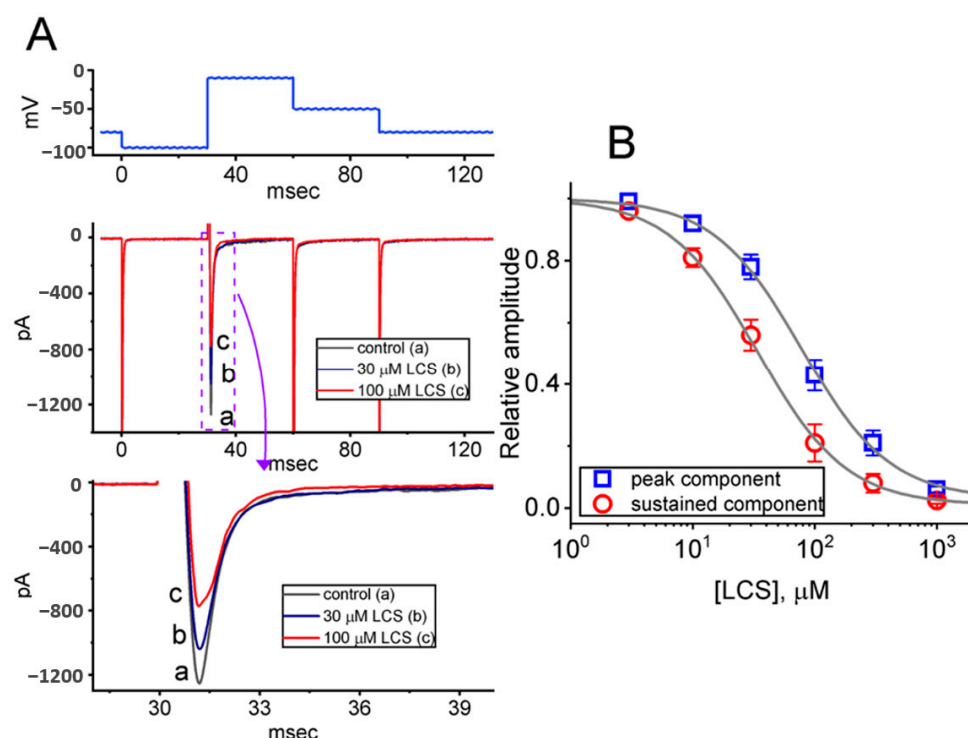


Figure 1. Effects of LCS on voltage-gated Na^+ current (I_{Na}) in GH₃ cells. **(A)** The top part shows the voltage-clamp protocol. The middle part is the representative current traces obtained in (a, black) the control period (i.e., no LCS) and in 30 μM LCS (b, blue) or 100 μM LCS (c, red). The bottom part represents the expanded record from the purple dashed box. **(B)** Concentration-dependent relationship of LCS on transient (peak component, open blue squares) and late (sustained component, open red circles) I_{Na} evoked by short membrane depolarization (mean \pm SEM; $n = 8$ for each point). The continuous gray line denotes the goodness-of-fit to a modified Hill equation, as stated in Section 4.

The inhibitory effects of LCS on I_{Na} were verified in another kind of excitable cell: Neuro-2a cells. LCS (30 or 100 μM) also suppressed both the amplitude of $I_{\text{Na(T)}}$ and $I_{\text{Na(L)}}$ elicited by the rapid membrane depolarization (Figure 2A). Figure 2B shows a differential dose-dependent response of LCS-induced suppression of $I_{\text{Na(T)}}$ and $I_{\text{Na(L)}}$ in Neuro-2a cells. Based on a modified Hill equation, the IC_{50} values to inhibit the $I_{\text{Na(T)}}$ and $I_{\text{Na(L)}}$ amplitude were 112 and 26 μM , respectively. Thus, LCS can suppress the magnitude of $I_{\text{Na(T)}}$ and $I_{\text{Na(L)}}$ in a time- and concentration-dependent manner both in GH₃ cells and Neuro-2a cells.

2.2. Effects of LCS on Persistent Na^+ Current ($I_{\text{Na(P)}}$) Triggered by Isosceles-Triangular Ramp Voltage (V_{ramp})

The persistent Na^+ current ($I_{\text{Na(P)}}$) is activated in the subthreshold voltage range and is also important in epilepsy by enhancing the repetitive firing capability of neurons. In this experiment, $I_{\text{Na(P)}}$ was elicited in GH₃ cells by an isosceles-triangular ramp voltage (V_{ramp}), which consisted of an upsloping (ascending) voltage from -100 mV to $+50$ mV followed by a downsloping (descending) voltage from $+50$ mV back to -100 mV in 1 s [29–31]. Voltage-dependent hysteresis (Hys_{V}) was observed in the instantaneous current–voltage (I – V) relationship of $I_{\text{Na(P)}}$ and presented as two distinct Hys_{V} loops of the I_{Na} amplitude: a high- (a counterclockwise direction) threshold loop and a low- (a clockwise direction) threshold loop (Figure 3A). Figure 3B shows the time course of the inhibitory effect of LCS (30 or 100 μM) on $I_{\text{Na(P)}}$ amplitudes activated by double V_{ramp} . Compared with the control situation without LCS, LCS reduced the $I_{\text{Na(P)}}$ amplitudes on the loop of Hys_{V} (Figure 3B,C). The 30 and 100 μM LCS attenuated the $I_{\text{Na(P)}}$ amplitudes at the level of -5 mV of the ascending limb to 245 ± 21 pA ($n = 8$, $p < 0.05$) and 212 ± 17 pA ($n = 8$, $p < 0.05$) from control values of 313 ± 24 pA ($n = 8$), and the $I_{\text{Na(P)}}$ amplitudes at the level

of -60 mV of the descending limb to 151 ± 14 pA ($n = 8, p < 0.5$) and 101 ± 11 pA ($n = 8, p < 0.05$) from control values of 198 ± 17 pA ($n = 8$), respectively. The attenuation of $I_{Na(P)}$ was reversed by application of tefluthrin (Tef, $10 \mu\text{M}$), which is an activator of I_{Na} [30].

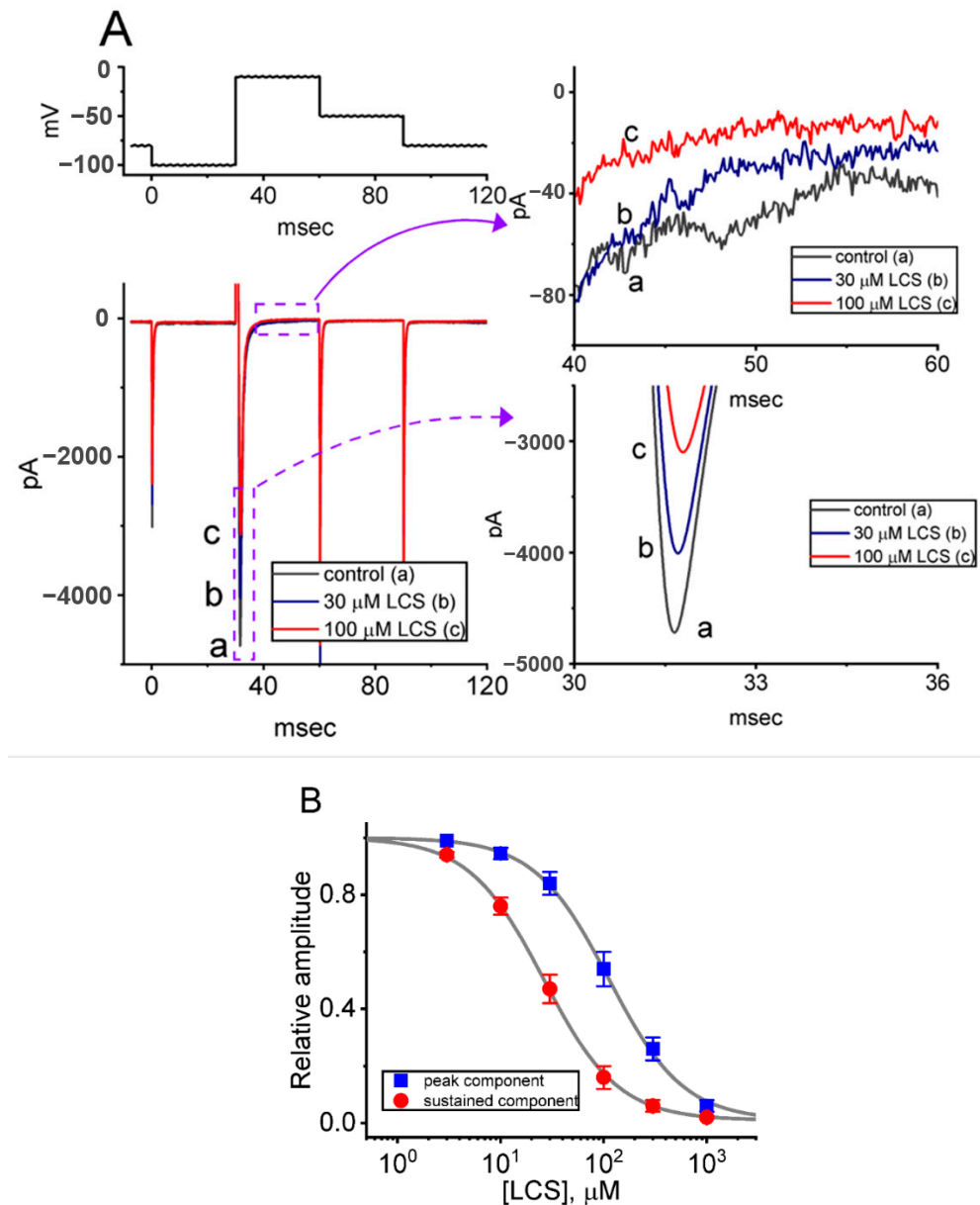


Figure 2. Effect of LCS on I_{Na} recorded from Neuro-2a cells. (A) The voltage-clamp protocol was on the top. The middle part was the representative current traces in response to depolarizing command pulses from -100 to -10 mV, a: control (i.e., no LCS, black); b: $30 \mu\text{M}$ LCS (blue); c: $100 \mu\text{M}$ LCS (red). The panels on the right side indicate the expanded records (i.e., $I_{Na(L)}$ and $I_{Na(T)}$) from each purple dashed box. (B) Dose-dependent relationship of LCS on $I_{Na(T)}$ (peak component, blue squares) and $I_{Na(L)}$ (sustained component, red circles) evoked by short membrane depolarization from -100 to -10 mV (mean \pm SEM; $n = 8$ for each point). The continuous gray line represents the best fit to a modified Hill equation, as described in Section 4.

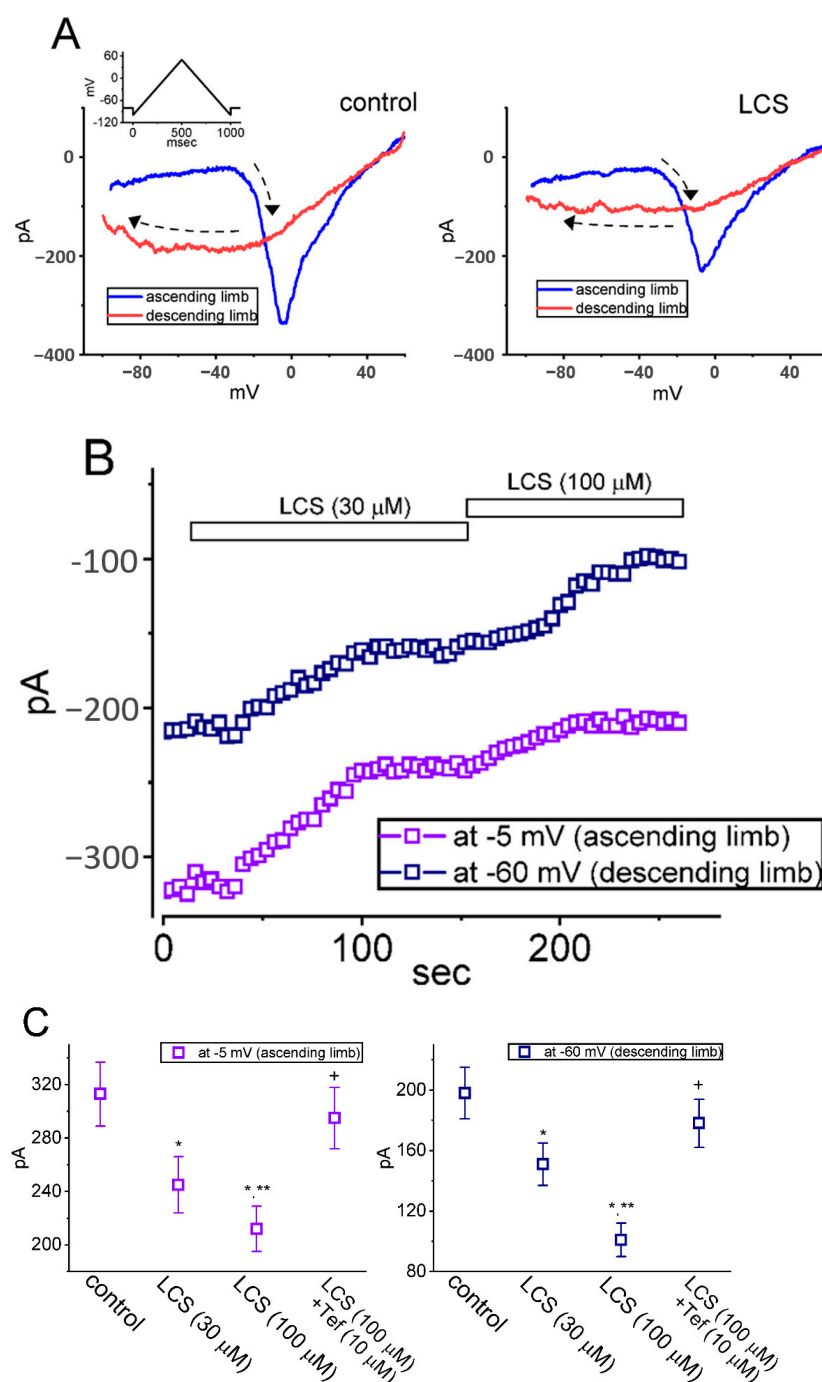


Figure 3. Inhibitory effect of LCS on persistent I_{Na} ($I_{Na(P)}$) activated by an isosceles-triangular ramp voltage (V_{ramp}) residing in GH₃ cells. **(A)** The voltage-clamp protocol of V_{ramp} is shown on the top. The blue or red color indicates the current trajectory at the ascending or descending limb of V_{ramp} , respectively. The dashed black arrow in each panel denotes the direction of the $I_{Na(P)}$ trajectory by which the time goes during elicitation by such upright isosceles-triangular V_{ramp} . **(B)** Time course of inhibitory effect of LCS (30 or 100 μ M) during double V_{ramp} . V_{ramp} was applied every 4 s, and $I_{Na(P)}$ (open square) at -5 mV (ascending limb) or -60 mV (descending limb) was then measured. The horizontal bar shown above indicates the addition of LCS (30 or 100 μ M). **(C)** Summary graphs demonstrating effects of LCS (30 or 100 μ M) and LCS (100 μ M) plus tefluthrin (Tef, 10 μ M) on I_{Na} amplitude activated by the upsloping (left, high-threshold $I_{Na(P)}$ at -5 mV) and downsloping (right, low-threshold $I_{Na(P)}$ at -60 mV) V_{ramp} (mean \pm SEM; $n = 8$ for each point). * Significantly different from controls ($p < 0.05$), ** significantly different from LCS (30 μ M)-alone group ($p < 0.05$), and + significantly different from LCS (100 μ M)-alone group ($p < 0.05$).

2.3. Effect of LCS on Window I_{Na} ($I_{Na(W)}$) Elicited by a Short Ascending V_{ramp}

The next question is if the magnitude of $I_{Na(W)}$ in response to the rapid ascending V_{ramp} can be modified by LCS. The instantaneous $I_{Na(W)}$ was evoked by an ascending V_{ramp} from -80 to $+40$ mV for 30 msec (i.e., a ramp speed of 4 mV/msec) [32,33]. As shown in Figure 4A, the amplitude of $I_{Na(W)}$ was markedly reduced within one minute while Neuro-2a cells were exposed to LCS. LCS (100 or 300 μ M) decreased the amplitude of $I_{Na(W)}$ measured at the level of -10 mV from a control value of 602 ± 27 pA ($n = 7$) to 442 ± 21 pA ($n = 7$, $p < 0.05$) or 296 ± 18 pA ($n = 7$, $p < 0.05$), respectively. After washout of LCS, the current amplitude at -10 mV was returned to 594 ± 24 pA ($n = 7$). Figure 4B illustrates a summary graph demonstrating the changes in Δ area of V_{ramp} -elicited $I_{Na(W)}$ measured at the voltage between -40 and $+40$ mV. It showed that LCS effectively diminished the $I_{Na(W)}$'s area and Tef (10 μ M) could reverse the LCS-mediated decrease in V_{ramp} -elicited $I_{Na(W)}$'s area.

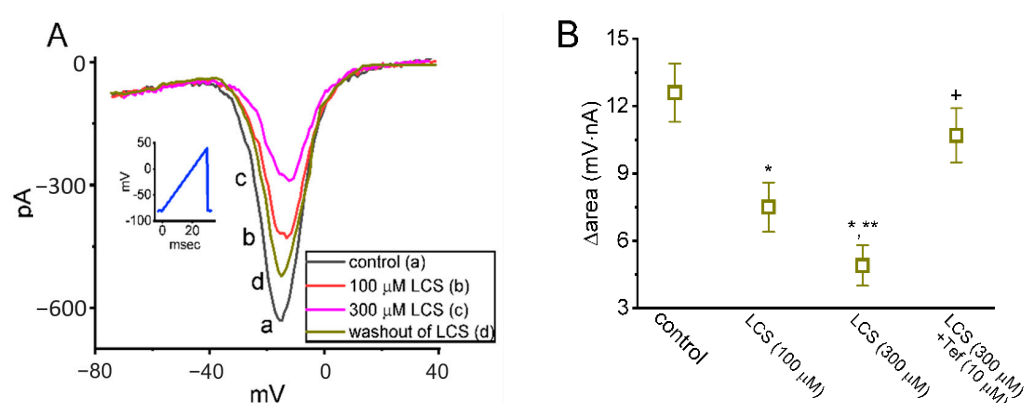


Figure 4. Modification by LCS of instantaneous window I_{Na} ($I_{Na(W)}$) evoked in response to short ascending V_{ramp} in Neuro-2a cells. **(A)** Representative current traces were acquired in the control period (a, black), during cell exposure to 100 μ M LCS (b, red) or 300 μ M LCS (c, pink), and washout of LCS (d, brown). The voltage protocol is illustrated in the inset, and the downward deflection indicates instantaneous inward current (i.e., $I_{Na(W)}$) elicited by a short ascending V_{ramp} . **(B)** Summary graph demonstrating attenuating effect of LCS (100 or 300 μ M) and LCS (300 μ M) plus Tef (10 μ M) on the Δ area of $I_{Na(W)}$ (mean \pm SEM; $n = 7$ for each point). Each area in this work was measured at the voltages ranging between -40 and $+40$ mV during the ascending V_{ramp} . * Significantly different from control ($p < 0.05$), ** significantly different from LCS (100 μ M) group ($p < 0.05$), and + significantly different from LCS (300 μ M) group ($p < 0.05$).

2.4. Effect of LCS on the Cumulative Inhibition of I_{Na} during a Train of Depolarizing Pulses

$I_{Na(T)}$ inactivation was previously demonstrated to accumulate before being activated during repetitive short pulses, which consisted of repetitive depolarization from -80 mV to -10 mV for 1 s with 40 msec in each pulse at a rate of 20 Hz [32,34]. To see the effects of LCS on the cumulative inhibition of I_{Na} , the $I_{Na(T)}$ or $I_{Na(L)}$ amplitude with or without treatment of LCS was simultaneously measured at the beginning or the end of each depolarizing pulse. Without LCS, the $I_{Na(T)}$ or $I_{Na(L)}$ inactivation evoked by a 1 s repetitive depolarization showed decaying τ values of 86 ± 9 or 234 ± 22 msec ($n = 8$), respectively (Figure 5). This indicates a pronounced time-dependent decay of $I_{Na(T)}$ or $I_{Na(L)}$, which can be fitted with a single-exponential process. Under 30 and 100 μ M LCS, the exponential time course of $I_{Na(T)}$ or $I_{Na(L)}$ elicited by the same train of depolarizing pulses was shortened to 64 ± 7 msec ($n = 8$, $p < 0.05$) and 31 ± 6 msec ($n = 8$, $p < 0.05$), or to 143 ± 9 msec ($n = 8$, $p < 0.05$) and 104 ± 6 msec ($n = 8$, $p < 0.05$), respectively. Thus, that accumulative inactivation of the current can be strikingly enhanced in the cells upon LCS exposure apart from a decrease in $I_{Na(T)}$ and $I_{Na(L)}$ amplitude.

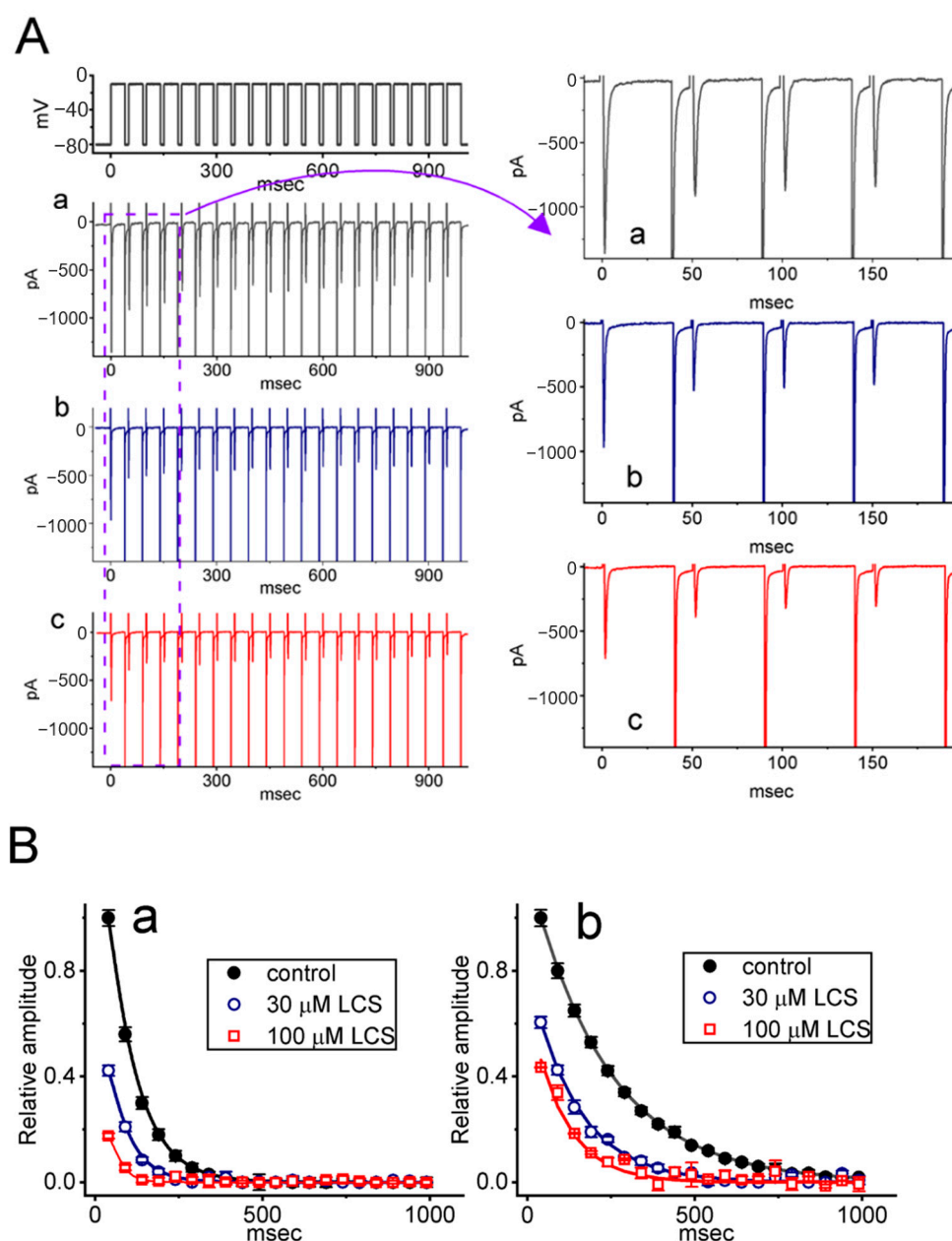


Figure 5. Effect of LCS on $I_{Na(T)}$ activated by a train of depolarizing pulses in GH₃ cells. The train consisted of twenty 40 msec pulses (stepped to -10 mV) separated by 10 msec intervals at -80 mV for 1 s. **(A)** Representative current traces were acquired in the control period ((a), no LCS, black) and during exposure to 30 μ M ((b), blue) or 100 μ M LCS ((c), red). The top part shows the voltage-clamp protocol applied. The right side of **(A)** represents the expanded records from the purple dashed box on the left side. **(B)** The relationship of the amplitude of $I_{Na(T)}$ ((a), **(left)**) or $I_{Na(L)}$ ((b), **(right)**) versus the pulse-train duration in the absence (black circles) and presence of 30 μ M LCS (open blue circles) or 100 μ M LCS (open red squares) was constructed (mean \pm SEM; $n = 8$ for each point). The $I_{Na(T)}$ or $I_{Na(L)}$ amplitude was measured at the beginning or end of each depolarizing step, respectively.

The effects of LCS on the cumulative inhibition of I_{Na} were also verified in Neuro-2a cells. Consistently, LCS (100 μ M) diminished the $I_{Na(T)}$ magnitude and decreased the decaying τ value of $I_{Na(T)}$ during repetitive depolarizations from a control value of 79 ± 9 msec to 39 ± 5 msec ($n = 7$, $p < 0.05$) (Figure 6A,B). In addition, the LCS-mediated reduction in decaying τ value of $I_{Na(T)}$ could be partially reversed by veratridine (Figure 6C).

Veratridine was a sodium channel agonist and was recently reported to modify the gating of the human NaV1.7 channel [35].

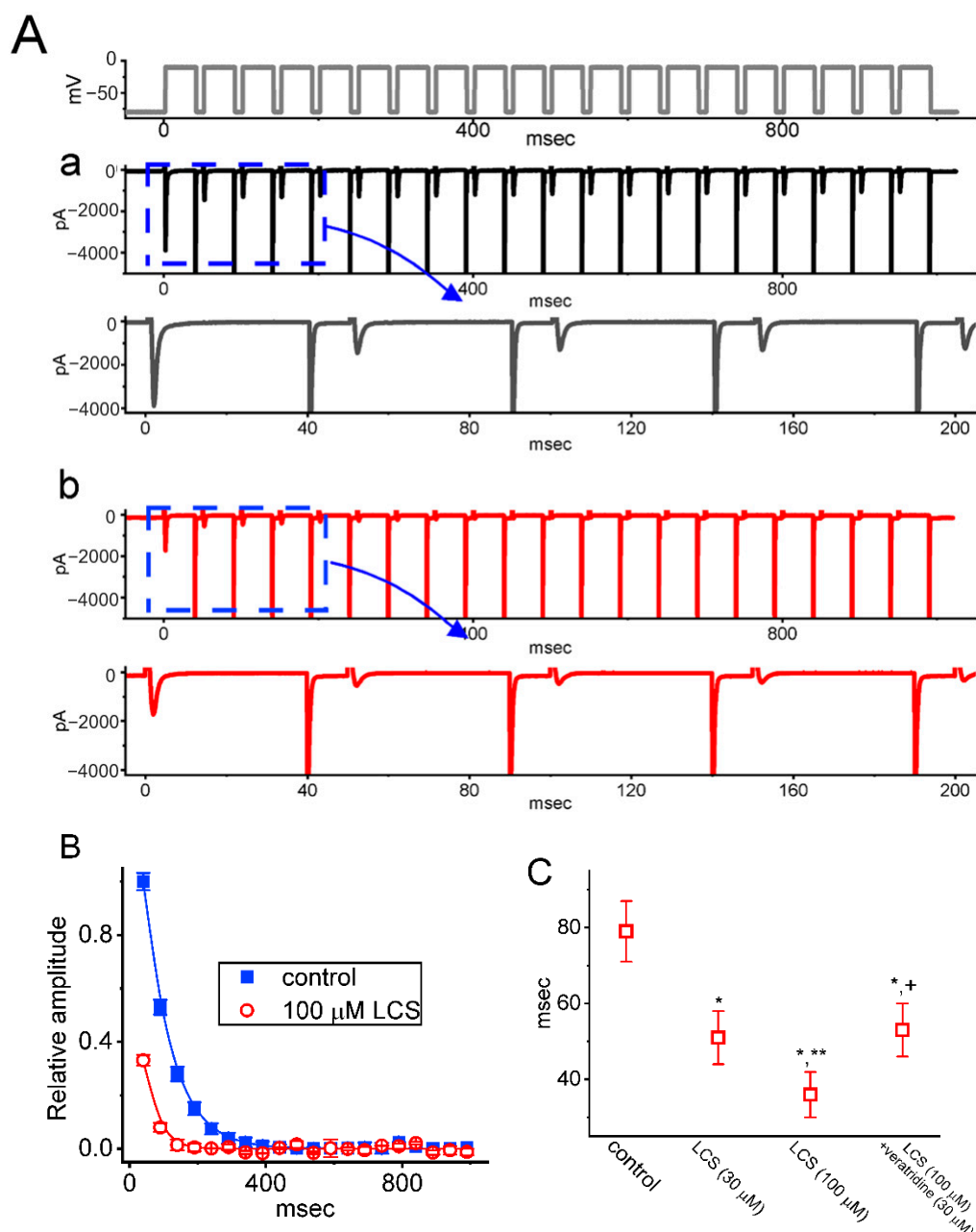


Figure 6. Effect of LCS on $I_{Na(T)}$ during a train of depolarizing pulses in Neuro-2a cells. **(A)** The top part is the voltage-clamp protocol. Representative current traces during the control period (a), black) or exposure to 100 μ M LCS (b), red) were presented. **(B)** The relationship of the relative amplitude of $I_{Na(T)}$ versus the pulse duration with (open red circles) or without (blue squares) LCS (100 μ M) (mean \pm SEM; $n = 7$ for each point). Each smooth line is well fitted to a single exponential. **(C)** Summary graph demonstrating the effect of LCS (30 or 100 μ M) and LCS (100 μ M) plus veratridine (30 μ M) on the τ value of $I_{Na(T)}$ during repetitive depolarizing pulses (mean \pm SEM; $n = 7$ for each point). * Significantly different from control ($p < 0.05$), ** significantly different from LCS (30 μ M)-alone group ($p < 0.05$), and + significantly different from LCS (100 μ M)-alone group ($p < 0.05$).

2.5. Modification by LCS of the Recovery Process of $I_{Na(T)}$ Inactivation following Conditioning Train of Depolarizing Stimuli

Earlier investigations have disclosed a unique type of recovery from $I_{Na(T)}$ inactivation evoked by a train of the preceding conditioning depolarizing stimuli [34,36,37]. The preceding conditioning train was composed of twenty 40 msec pulses separated by 5 msec intervals at -80 mV for 1 s (Figure 7A, top). Following such a conditioning train, the I_{Na} was produced by a two-step voltage protocol to measure the recovery time course of the current. The two-step voltage protocol included the first step that consisted of a 30 msec pulse from -80 to -10 mV and a second step that consisted of pulses for a variable length of time in a geometric progression (common ratio = 2) from -80 to -10 mV. The relative amplitude of recovery for current inactivation during this protocol was determined by the second step.

Table 1. Summary of data demonstrating the parameter values for the modulatory effect of LCS on the recovery of I_{Na} block during the preceding train pulse observed in pituitary GH3 cells. These parameters are elaborated in detail in Section 4.

	N	τ_{fast} (msec)	τ_{slow} (msec)	A	B
Control	8	12.2 ± 0.4	885 ± 16	0.71 ± 0.04	0.28 ± 0.02
LCS (30 μ M)	8	$13.6 \pm 0.6^*$	$972 \pm 17^*$	$0.78 \pm 0.04^*$	$0.22 \pm 0.02^*$
LCS (100 μ M)	8	$14.1 \pm 0.6^*$	$1045 \pm 19^*$	$0.81 \pm 0.04^*$	$0.18 \pm 0.02^*$

All values are mean \pm SEM. * Significantly different from controls ($p < 0.05$).

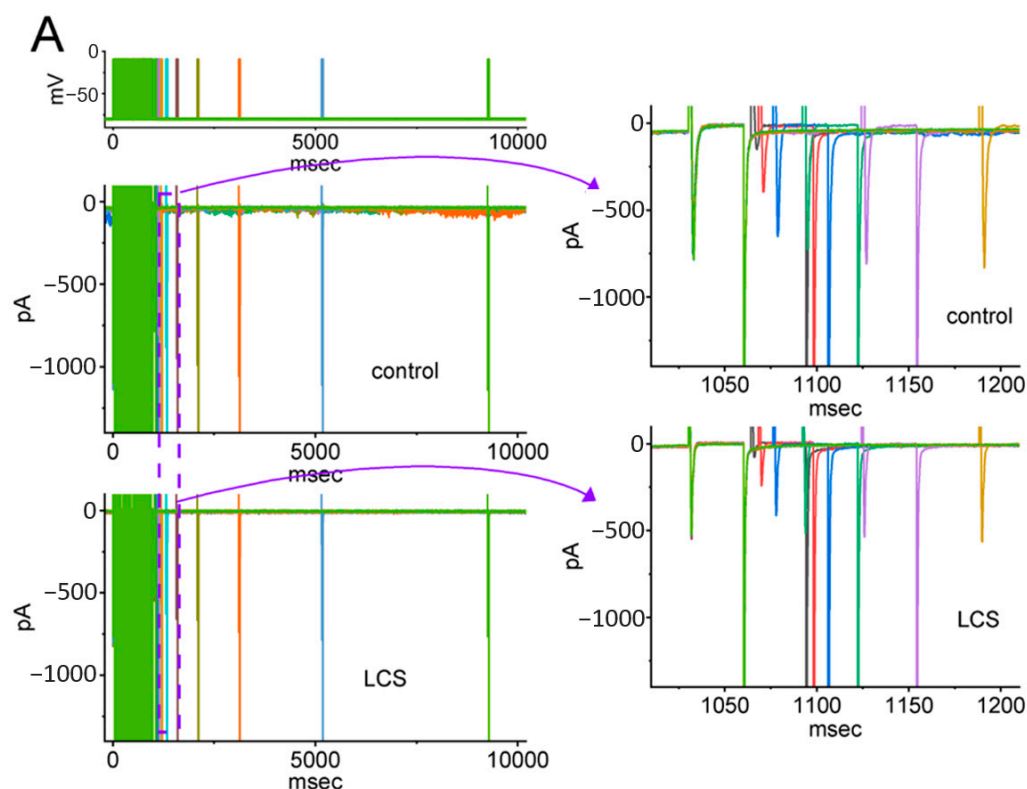


Figure 7. Cont.

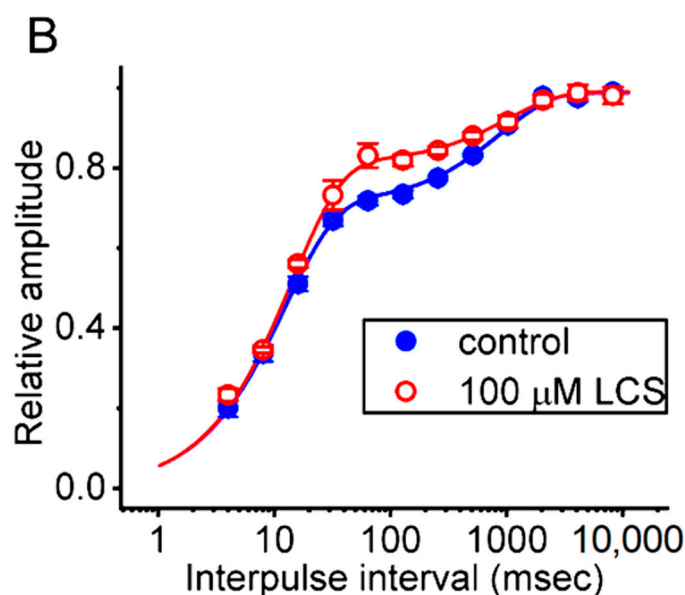


Figure 7. The recovery of I_{Na} inactivation during the train of conditioning depolarizing pulses modified by the presence of LCS. (A) The voltage-clamp protocol is shown on the top. Representative current traces were taken in the control period (middle part) and during exposure to 100 μ M LCS (lower part). The right side of (A) denotes the expanded records from the purple dashed box on the left side. (B) The relationship of the relative amplitude of $I_{Na(T)}$ versus the interpulse interval was obtained in the absence (blue circles) and presence (open red circles) of 100 μ M LCS (mean \pm SEM; $n = 8$ for each point). The blue or red smooth curve taken with or without the application of LCS was least-squares fitted with a two-exponential function, as detailed in Section 4, while the parameters are illustrated in Table 1.

In the control situation (i.e., without LCS), the recovery from $I_{Na(T)}$ inactivation elicited by the preceding conditioning depolarizing stimuli was noticed to emerge in a biphasic manner including a rapid rising recovery phase followed by a late slow phase (Figure 7A). It indicates a train of stimuli enabling the cells to resist the recovery from $I_{Na(T)}$ inactivation. The recovery time course of this biphasic-manner $I_{Na(T)}$ inactivation was constructed in Figure 7B. The experimental data points were well fitted with a sum of two exponential functions, i.e., fast (τ_{fast}) and slow time constant (τ_{slow}), as elaborated in Materials and Methods. Upon exposure to LCS (30 or 100 μ M), both τ_{fast} and τ_{slow} in the recovery time course of current inactivation was increased ($p < 0.05$) compared to the control situation (Table 1).

3. Discussion

The principal finding in this study was that LCS could suppress I_{Na} in a time-, concentration- and frequency-dependent manner identified in GH₃ and Neuro-2 cells. LCS induced differential inhibitions of $I_{Na(T)}$ and $I_{Na(L)}$ activated by a short depolarizing pulse. It also suppressed the high- or low-threshold amplitude of $I_{Na(P)}$ elicited by the upright isosceles-triangular V_{ramp} at either the upsloping or downsloping limb leading to a striking reduction in $Hys_{(V)}$ strength of the current. The accumulative inhibition of $I_{Na(T)}$ and $I_{Na(L)}$ during a train of depolarizing pulses was substantially enhanced by LCS, and the values of τ_{fast} and τ_{slow} in the recovery time course during the preceding conditioning train of depolarizing pulses were increased. Taken together, LCS could modify the magnitude, gating properties, use-dependence, and $Hys_{(V)}$ behaviors of I_{Na} , leading to the inhibition of $I_{Na(T)}$, $I_{Na(L)}$, $I_{Na(P)}$, and $I_{Na(W)}$.

In the present investigations, the non-equilibrium voltage-dependent hysteresis ($Hys_{(V)}$) of $I_{Na(P)}$ was observed by an upright isosceles-triangular V_{ramp} with a duration of 1 s (Figure 3). This implies that the $I_{Na(P)}$ magnitude is contingent on the pre-existing state(s) or

conformation(s) of the Na_V channel. There are two types of triangular V_{ramp}-elicited $I_{Na(P)}$, that is, low-threshold (i.e., activated at a voltage range near the resting potential) elicited upon the downsloping end of the triangular V_{ramp}, and high-threshold (i.e., activated at a voltage range near the maximal $I_{Na(T)}$) elicited on the upsloping end of such V_{ramp} [28]. LCS attenuated both types of triangular V_{ramp}-elicited $I_{Na(P)}$ of the Hys_(V) behaviors and Tef could effectively reverse this LCS-induced reduction in Hys_(V)'s strength in the current. In the literature, this Hys_(V) behavior of triangular V_{ramp}-elicited $I_{Na(P)}$ has been demonstrated to link to the magnitude of background Na⁺ currents closely, and $I_{Na(L)}$ and $I_{Na(P)}$ during an extended period of time are likely to share the same Na_V channels [29,31,34,38,39]. This result indicates that LCS could diminish the background Na⁺ currents conductance and reduce the subthreshold potential or depolarization drive in these excitable cells.

In addition, the time-dependent decline in $I_{Na(T)}$ and $I_{Na(L)}$ during a 20 Hz train of depolarizing voltage commands (i.e., 40 msec pulses applied from −80 to −10 mV at a rate of 20 Hz for 1 sec) was observed in an exponential fashion, as shown in Figures 5 and 6. This accumulative inhibition is a use-dependent property of $I_{Na(T)}$ and $I_{Na(L)}$ during rapid repetitive stimuli or high-frequency firing [32,34,40–43]. LCS could enhance this accumulative inhibition through reducing not only the amplitude but also the τ value of $I_{Na(T)}$ and $I_{Na(L)}$. The LCS-mediated enhancement was only reversed partially by veratridine, a sodium channel agonist. This means that LCS would lead to a “loss-of-function” change of Na⁺ channels and keep the Na⁺ channels in inactivated states during repetitive depolarization to prevent excessive excitability. In addition to LCS, a recent study demonstrated that other sodium blockers, such as lidocaine, also had the use-dependent inhibition of corneal nerve activity [44]. It is consistent with the current investigations.

It is important to emphasize that the LCS increased the τ_{fast} and τ_{slow} of recovery from the $I_{Na(T)}$ block elicited by the preceding conditioning train pulse and enlarged the value of A, as summarized in Table 1. This preceding conditioning train pulse consisted of rapid repetitive pulses, which mimics high-frequency firing on excitable cells and would cause a large fraction of Na_V channels to shift toward the slowly recovering pool. The value of A indicates the fraction of the slow recovering pool of Na_V channels. Taken together, LCS could cause a larger fraction of the Na_V channels in an inactivated state and a longer recovery from inactivation after rapid repetitive stimuli or high-frequency firing. These results are partly relevant to the previous study that showed slow inactivation enhancement by LCS [21].

In this work, we further investigated how the protein of Na_V could be delicately docked with LCS by using PyRx software (<https://sourceforge.net/projects/pyrx/>; accessed on 17 July 2022). The predicted binding sites with LCS are demonstrated in Figure 8. The LCS could form hydrophobic contacts with several residues, including Gly 76, Trp 77, Phe 80, Gln 122, Leu 125, and Leu 126. Phe 80 can interact with the N'-acetyl amino acid N'-benzyl amide unit of LCS, Gly 76 and Trp 77 can dock to the linker that connects the two-aryl group, while Gln 122, Leu 125, and Leu 126 are noted to interact with the terminal aromatic ring. These three functional groups (i.e., N'-acetyl amino acid N'-benzyl amide unit, the linker that connects the two aryl groups, and the terminal aromatic ring) in the molecule could be essential for its Na_V-channel blocking activity [7]. However, as the 4' position of the structural moiety in safinamide (α -aminoamide) does not affect the slow inactivation of Na_V channels, the interaction with Phe 80 appears to be unimportant. The detailed structure of this Na_V channel, which is a particularly good exemplar for hNa_V pharmacology, was shown in an earlier study [45]. These results indicate that LCS can favorably interact with the amino-acid residues of the Na_V channel with an estimated binding affinity of −5.0. Kcal/mol, which is adjacent to the transmembrane region (i.e., position: 123–148) or membrane segment (i.e., position: 79–95) of the channel. Consequently, when LCS reaches the Na_V channels on the membrane, the interactions may raise the structural or steric constraints, thereby resulting in a substantial decrease in Na_V-channel openings.

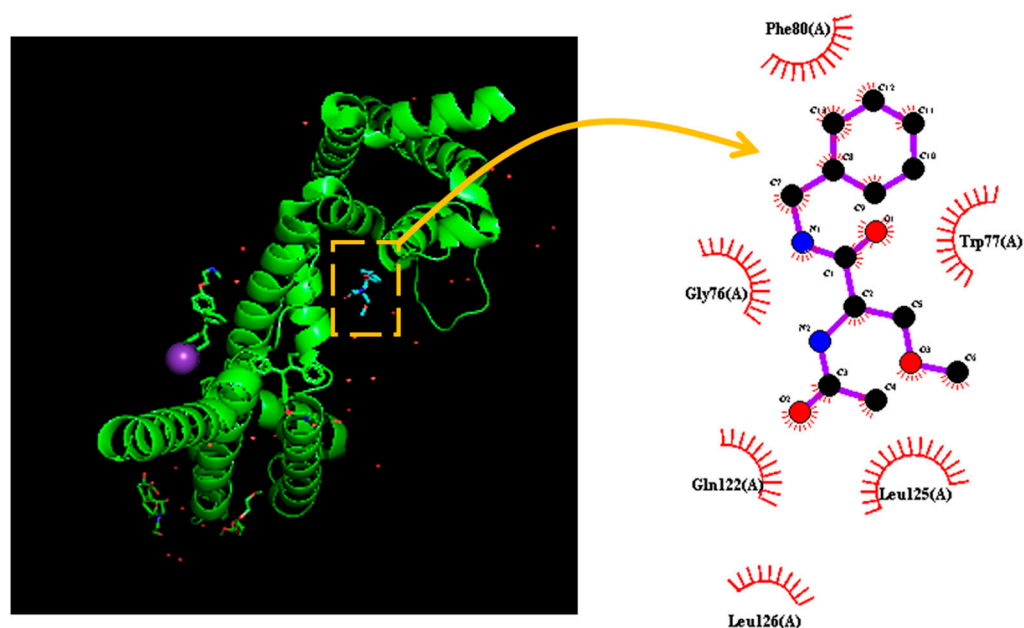


Figure 8. Predicted docking results demonstrating an interaction with Na_v channel and lacosamide (LCS). The protein structure of the Na_v (SCN) channel was acquired from PDB (PDB ID: 6Z8C), while the chemical structure of LCS was from PubChem (Compound CID: 219078). The structure of the Na_v channel was docked with the LCS molecule through PyRx (<https://pyrx.sourceforge.io/>, accessed on 5 June 2022). The diagram of the interaction between Na_v and the LCS molecule was generated by LigPlot⁺ (<https://www.ebi.ac.uk/thornton-srv/software/LIGPLOT/>, accessed on 15 June 2022). Note that the red arcs with spokes that radiate toward the ligand (i.e., LCS, in the center) represent the hydrophobic contacts.

In summary, LCS could suppress I_{Na} in a time-, concentration-, and frequency-dependent manner and modify the magnitude, gating properties, use-dependence, and $Hys_{(V)}$ behaviors of I_{Na} , leading to inhibiting $I_{Na(T)}$, $I_{Na(L)}$, $I_{Na(P)}$, and $I_{Na(W)}$. Consequently, LCS could reduce the subthreshold potential, enhance the accumulative inhibition during repetitive depolarization, and prolong the recovery from inactivation after repetitive depolarization in excitable cells.

4. Materials and Methods

4.1. Chemicals, Drugs, and Solutions Used in This Study

Lacosamide (LCS, Vimpat[®], *R*-enantiomer of 2-acetamido-*N*-benzyl-3-methoxy-propionamide, 2,3-diaminomaleonitrile, C₁₃H₁₈N₂O₃), tefluthrin (Tef), tetraethylammonium chloride (TEA), tetrodotoxin (TTX), and veratridine were supplied by Sigma-Aldrich (Merck, Taipei, Taiwan). For cell preparations, we obtained culture media, fetal bovine or calf serum, horse serum, L-glutamine, and trypsin/EDTA from HyClone[™] (Thermo Fisher, Kaohsiung, Taiwan). All other chemicals used in this work (e.g., CsOH, CsCl, CdCl₂, and HEPES) were of laboratory grade and taken from standard sources. Double-distilled water deionized through a Milli-Q[®] purification system (Merck, Tainan, Taiwan) was used in all experiments.

The ionic composition of normal Tyrode's solution buffered by HEPES was as follows (in mM): NaCl 136.5, CaCl₂ 1.8, KCl 5.4, MgCl₂ 0.53, glucose 5.5, and HEPES-NaOH buffer (pH 7.4). During the measurements recording K⁺ currents, a patch electrode was filled with a solution (in mM): K-aspartate 130, KCl 20, MgCl₂ 1, KH₂PO₄ 1, Na₂ATP 0.1, Na₂GTP 0.1, EGTA 0.1, and HEPES-KOH buffer (pH 7.2). To measure different patterns of voltage-gated Na⁺ current, we substituted K⁺ ions in the internal solution for equimolar Cs⁺ ions, and the pH value in the solution was adjusted to 7.2 by adding CsOH. The pipette solution and

culture media presently used were filtered with an Acrodisc® syringe filter that contains a 0.2 µm Supor® nylon membrane (#4612; Pall Corp.; Genechain, Kaohsiung, Taiwan).

4.2. Cell Preparations

Both the mouse neuroblastoma cell line, Neuro-2a (N2a, BCRC-60026), and the pituitary adenomatous cell line, GH₃ (BCRC-60015), were acquired from the Bioresource Collection and Research Center (Hsinchu, Taiwan). GH₃ cells were in Ham's F medium supplemented with 2.5% (*v/v*) fetal calf serum, 15% (*v/v*) horse serum, and 2 mM L-glutamine, while Neuro-2a cells were in Dulbecco's modified Eagle's medium with 10% (*v/v*) fetal bovine serum. These cells were maintained at 5% CO₂ in a 37 °C water-jacketed incubator. Growth medium was replaced twice a week, and cells were split into subcultures once a week. Subcultures were made with trypsinization (0.025% trypsin solution (HyClone™) containing 0.01% sodium *N*, *N*-diethyldithiocarbamate and EDTA). Electrophysiological measurements were undertaken five or six days after cells were cultured up to 60–80% confluence [30].

4.3. Electrophysiological Measurements

During the few hours before the measurements, we harvested Neuro-2a or GH₃ cells with 1% trypsin-EDTA solution, and a few drops of cell suspension were rapidly placed into a custom-built recording chamber fixed on the stage of an inverted DM-IL microscope (Leica; Major Instruments, Tainan, Taiwan). We then suspended cells at room temperature (20–25 °C) in normal Tyrode's solution until cells attached to the chamber's bottom before the recordings were made. The pipettes used were fabricated from Kimax-51 glass tubing with an 1.5–1.8 mm outer diameter (#34500; Kimble, Dogger, New Taipei City, Taiwan) with a vertical two-stage puller (PP-83; Narishige, Taiwan Instrument, Tainan, Taiwan). When filled with different internal solutions, the electrodes presently used for measurements had a tip resistance of 3–5 MΩ. Ionic currents were examined in the whole-cell configuration of a modified patch-clamp technique with the use of either an Axoclamp-2B (Molecular Devices, Sunnyvale, CA, USA) or an RK-400 amplifier (Bio-Logic, Claix, France), as described elsewhere [28]. GΩ-seals were achieved in an all-or-nothing fashion and resulted in a dramatic improvement in the signal-to-noise ratio. The liquid junction potentials, which occur when the compositions in bath solution and those of the pipette internal solution are different, became zeroed shortly before GΩ-seal formation was achieved, and the whole-cell data were then corrected as previously described [30].

4.4. Data Recordings

The signals were monitored and digitally captured and stored online at 10 kHz or more in an ASUS ExpertBook laptop computer (Yuan-Dai, Tainan, Taiwan). For efficient analog-to-digital (A/D) and digital-to-analog (D/A) conversion to proceed, a Digidata®-1440A digitizer connected with a laptop computer via a USB 2.0 port was delicately operated by pClamp 10.6 software run under Microsoft Windows 7 (Redmond, WA, USA). Amplified current signals were low-pass-filtered at 2 kHz with an FL-4 four-pole Bessel filter (Dagan, Minneapolis, MN, USA). The voltage-clamp protocols comprising various rectangular and ramp waveforms were specifically designed and were thereafter imposed on the tested cells through D/A conversion. As pulse-train stimulation was needed, we used a dual output pulse stimulator (Astro-Med Grass S88X; Grass, West Warwick, RI, USA).

4.5. Data Analyses

To assess the dose–response curve of LCS-mediated inhibition on the peak (transient, $I_{Na(T)}$) and sustained (late, $I_{Na(L)}$) components of depolarization-activated I_{Na} present in GH₃ or Neuro-2a cells, I_{Na} 's were evoked by a 30 msec depolarizing pulse to −10 mV from a holding potential of −100 mV (indicated in the top part of Figures 1A and 2A), and current amplitudes obtained with or without the exposure to different LCS concentrations (3 µM–1 mM) were measured at the beginning ($I_{Na(T)}$) and end ($I_{Na(L)}$) of the depolarizing

pulses. The concentration needed to suppress 50% of the current amplitude (i.e., IC_{50}) was appropriately determined according to the three-parameter logistic model (i.e., a modified form of the sigmoidal Hill equation) by use of goodness-of-fit assessments:

$$Relative\ amplitude = \frac{[LCS]^{-n_H} \times (1 - a)}{([LCS]^{-n_H} + IC_{50}^{-n_H})} + a \quad (1)$$

In this equation, $[LCS]$ = the LCS concentration; n_H = the Hill coefficient; IC_{50} = the concentration required for a 50% inhibition. Maximal inhibition (i.e., $1 - a$) was also approximated in this formula.

By a two-step voltage protocol with varying interpulse intervals in a geometric progression (common ratio = 2), the recovery time course of $I_{Na(T)}$ from the block activated in response to the 1 sec conditioning pulse train was constructed, and the results acquired with or without the addition of LCS to GH₃ or Neuro-2a cells were thereafter drawn by plotting the relative $I_{Na(T)}$ amplitude (normalized with respect to the steady-state amplitude activated at 0.1 Hz). A basic assumption of the analyses is that the recovery time course of the current established under these experimental conditions can be reliably described by an exponential function [34]. Because the recovery time course in GH₃ cells exhibits a rapid rising recovery phase followed by a late slow phase, there should be at least two underlying exponential terms. Accordingly, the data points showing a recovery time course with or without the addition of LCS were fitted to the exponential function with the biexponential process, i.e.,

$$y = A \times \left(1 - e^{-\frac{t}{\tau_{fast}}}\right) + B \times \left(1 - e^{-\frac{t}{\tau_{slow}}}\right) \quad (2)$$

where y is the relative amplitude of I_{Na} at time t , A or B is the relative amplitude of each exponential component, and τ_{fast} or τ_{slow} is the fast or slow time constant in the recovery of I_{Na} block, respectively.

4.6. Curve-Fitting Approximations and Statistical Analyses

Linear or nonlinear curve fitting to experimental datasets in this work was made with the interactive least-squares procedure by using various tools, such as Microsoft Excel[®]-embedded “Solver” (Microsoft, Redmond, WA, USA) and the OriginPro[®] 2021 program (OriginLab[®]; Scientific Formosa, Kaohsiung, Taiwan). The averaged results are presented as the mean \pm standard error of the mean (SEM) with the sizes of independent samples (n) indicating cell numbers from which data were taken. The Student’s t -test (paired or unpaired) between the two different groups was applied. When differences among more than two groups were encountered, we performed either analysis of variance (ANOVA)-1 or ANOVA-2 with or without repeated measures, followed by the post hoc Fisher’s least significant difference test. Statistical significance (indicated with *, **, or + in the figures) was determined at a p value of <0.05 .

Author Contributions: Conceptualization, S.-N.W., Y.-C.L., P.-M.W., C.-W.C. and Y.-F.T.; methodology, S.-N.W. and H.-Y.C.; software, H.-Y.C. and S.-N.W.; validation, H.-Y.C., T.-H.C. and M.-C.Y.; formal analysis, S.-N.W.; investigation, P.-M.W., H.-Y.C., T.-H.C., M.-C.Y., C.-W.C. and S.-N.W.; resources, S.-N.W.; data curation, Y.-C.L., C.-W.C. and S.-N.W.; writing—original draft preparation, S.-N.W., P.-M.W., Y.-C.L. and Y.-F.T.; writing—review and editing, S.-N.W., C.-W.C. and Y.-F.T.; project administration, S.-N.W., C.-W.C. and Y.-F.T.; funding acquisition, S.-N.W. and Y.-F.T. All authors have read and agreed to the published version of the manuscript.

Funding: This research was funded by the Ministry of Science and Technology (MOST-108-2314B-006-094; 110-2314-B-006-049; 110-2314-B-006-056; 111-2314-B-006-082) of Taiwan, and National Cheng Kung University Hospital (NCKUH-11102050; NCKUH-11102029).

Institutional Review Board Statement: Not applicable.

Informed Consent Statement: Not applicable.

Data Availability Statement: The original data are available upon reasonable request to the corresponding author.

Acknowledgments: The authors are grateful to Tzu-Hsien Chuang for the assistance.

Conflicts of Interest: The authors declare that they have no conflict of interest, financial or otherwise. The authors are responsible for the content of writing of the paper.

Abbreviations

Hys _(V)	voltage-dependent hysteresis
IC ₅₀	concentration required for 50% inhibition
I _{Na}	voltage-gated Na ⁺ current
I _{Na(L)}	late Na ⁺ current
I _{Na(P)}	persistent Na ⁺ current
I _{Na(T)}	transient (peak) Na ⁺ current
I _{Na(W)}	window Na ⁺ current
LCS	lacosamide (Vimpat [®])
Na _V channel	voltage-gated Na ⁺ channel
SEM	standard error of mean
τ	time constant
τ _{fast}	fast time constant
τ _{slow}	slow time constant
TEA	tetraethylammonium chloride
Tef	tefluthrin
TTX	tetrodotoxin
V _{ramp}	ramp voltage

References

- Labau, J.I.R.; Estacion, M.; Tanaka, B.S.; De Greef, B.T.A.; Hoeijmakers, J.G.J.; Geerts, M.; Gerrits, M.M.; Smeets, H.J.M.; Faber, C.G.; Merkies, I.S.J.; et al. Differential effect of lacosamide on Nav1.7 variants from responsive and non-responsive patients with small fibre neuropathy. *Brain* **2020**, *143*, 771–782. [\[CrossRef\]](#) [\[PubMed\]](#)
- Casciato, S.; Quarato, P.P.; Gialluisi, A.; D'Aniello, A.; Mascia, A.; Grammaldo, L.G.; Di Gennaro, G. Lacosamide as first add-on or conversion monotherapy: A retrospective real-life study. *Epilepsy Behav.* **2021**, *122*, 108128. [\[CrossRef\]](#) [\[PubMed\]](#)
- Eilam, A.; Khmeliov, N.; Penker, D.; Gilad, R. Intravenous Lacosamide in Seizure Clusters: Dose and Efficacy. *Clin. Neuropharmacol.* **2021**, *44*, 85–88. [\[CrossRef\]](#) [\[PubMed\]](#)
- Shin, Y.-W.; Moon, J.; Cho, Y.W.; Kim, D.W.; Bin Hong, S.; Kim, D.-Y.; Chang, H.; Yoon, S.H.; Yu, K.-S.; Jang, I.-J.; et al. Tolerability of lacosamide rapid dose titration: A randomized, multicenter, prospective, open-label study. *Epilepsy Behav.* **2021**, *115*, 107663. [\[CrossRef\]](#) [\[PubMed\]](#)
- Muñoz-Vendrell, A.; Teixidor, S.; Sala-Padró, J.; Campoy, S.; Huerta-Villanueva, M. Intravenous lacosamide and phenytoin for the treatment of acute exacerbations of trigeminal neuralgia: A retrospective analysis of 144 cases. *Cephalalgia* **2022**, *42*, 3331024221092435. [\[CrossRef\]](#) [\[PubMed\]](#)
- Scott, L.J. Lacosamide: A Review in Focal Seizures in Patients with Epilepsy. *Drugs* **2015**, *75*, 2143–2154. [\[CrossRef\]](#) [\[PubMed\]](#)
- Wang, Y.; Wilson, S.M.; Brittain, J.M.; Ripsch, M.S.; Salomé, C.; Park, K.D.; White, F.A.; Khanna, R.; Kohn, H. Merging Structural Motifs of Functionalized Amino Acids and α-Aminoamides Results in Novel Anticonvulsant Compounds with Significant Effects on Slow and Fast Inactivation of Voltage-gated Sodium Channels and in the Treatment of Neuropathic Pain. *ACS Chem. Neurosci.* **2011**, *2*, 317–322. [\[CrossRef\]](#)
- Biton, V. Lacosamide for the treatment of diabetic neuropathic pain. *Expert Rev. Neurother.* **2008**, *8*, 1649–1660. [\[CrossRef\]](#)
- McCleane, G. Lacosamide for pain. *Expert Opin. Investig. Drugs* **2010**, *19*, 1129–1134. [\[CrossRef\]](#) [\[PubMed\]](#)
- Hearn, L.; Derry, S.; Moore, R.A. Lacosamide for neuropathic pain and fibromyalgia in adults. *Cochrane Database Syst. Rev.* **2012**, *2012*, Cd009318. [\[CrossRef\]](#)
- Carmland, M.E.; Kreutzfeldt, M.; Holbech, J.V.; Andersen, N.T.; Jensen, T.S.; Bach, F.W.; Sindrup, S.H.; Finnerup, N.B. Effect of lacosamide in peripheral neuropathic pain: Study protocol for a randomized, placebo-controlled, phenotype-stratified trial. *Trials* **2019**, *20*, 588. [\[CrossRef\]](#) [\[PubMed\]](#)
- Adamo, D.; Coppola, N.; Pecoraro, G.; Nicolò, M.; Mignogna, M.D. Lacosamide in trigeminal neuralgia: Report of a case refractory to first- and second-generation anticonvulsants. *Cranio* **2020**, 1–5. [\[CrossRef\]](#)
- Huang, C.-W.W.; Brown, S.; Pillay, N.; Del Campo, M.; Tellez-Zenteno, J.; McLachlan, R.S. Electroencephalographic and Electrocardiographic Effect of Intravenous Lacosamide in Refractory Focal Epilepsy. *J. Clin. Neurophysiol.* **2018**, *35*, 365–369. [\[CrossRef\]](#)

14. Wu, T.; Chuang, Y.C.; Huang, H.C.; Lim, S.N.; Hsieh, P.F.; Lee, W.T.; Cheng, M.-Y.; Tsai, M.-H.; Jou, S.-B.; Chang, C.-W.; et al. A prospective, multicenter, noninterventional study in Taiwan to evaluate the safety and tolerability of lacosamide as adjunctive therapy for epilepsy in clinical practice. *Epilepsy Behav.* **2020**, *113*, 107464. [[CrossRef](#)] [[PubMed](#)]
15. Nortey, J.; Smith, D.; Seitzman, G.D.; Gonzales, J.A. Topical Therapeutic Options in Corneal Neuropathic Pain. *Front. Pharmacol.* **2021**, *12*, 769909. [[CrossRef](#)]
16. Okanishi, T.; Fujii, Y.; Sakuma, S.; Shiraishi, H.; Motoi, H.; Yazaki, K.; Enoki, H.; Fujimoto, A. Lacosamide monotherapy for the treatment of childhood epilepsy with centropetal spikes. *Brain Dev.* **2022**, *44*, 380–385. [[CrossRef](#)]
17. Panda, P.K.; Sharawat, I.K.; Dawman, L.; Panda, P.; Kasinathan, A.; Rathaur, V.K. Efficacy and Tolerability of Lacosamide in Lennox-Gastaut Syndrome: A Systematic Review and Meta-analysis. *J. Neurosci. Rural. Pract.* **2022**, *13*, 32–42. [[CrossRef](#)]
18. Pozzi, M.; Zanotta, N.; Epifanio, R.; Baldelli, S.; Cattaneo, D.; Clementi, E.; Zucca, C. Lacosamide effectiveness and tolerability in patients with drug-resistant epilepsy and severe disability under polytherapy: Therapy optimization as emerging from an observational study. *Epilepsy Behav.* **2022**, *128*, 108598. [[CrossRef](#)]
19. Ragoonanan, D.; Tran, N.; Levesque, M. Safety and Tolerability of Intravenous Push Lacosamide and Levetiracetam. *J. Pharm. Pract.* **2022**, 8971900221087955. [[CrossRef](#)]
20. Behr, C.; Lévesque, M.; Ragsdale, D.; Avoli, M. Lacosamide modulates interictal spiking and high-frequency oscillations in a model of mesial temporal lobe epilepsy. *Epilepsy Res.* **2015**, *115*, 8–16. [[CrossRef](#)]
21. Errington, A.C.; Stohr, T.; Heers, C.; Lees, G. The investigational anticonvulsant lacosamide selectively enhances slow inactivation of voltage-gated sodium channels. *Mol. Pharmacol.* **2008**, *73*, 157–169. [[CrossRef](#)] [[PubMed](#)]
22. Wang, G.K.; Wang, S.-Y. Block of human cardiac sodium channels by lacosamide: Evidence for slow drug binding along the activation pathway. *Mol. Pharmacol.* **2014**, *85*, 692–702. [[CrossRef](#)] [[PubMed](#)]
23. Rogawski, M.A.; Tofighy, A.; White, H.S.; Matagne, A.; Wolff, C. Current understanding of the mechanism of action of the antiepileptic drug lacosamide. *Epilepsy Res.* **2015**, *110*, 189–205. [[CrossRef](#)] [[PubMed](#)]
24. Sumbul, O.; Aygun, H. Electrocardiographic and electrocardiographic evaluation of lacosamide in a penicillin-induced status epilepticus model. *Epilepsy Res.* **2022**, *180*, 106866. [[CrossRef](#)] [[PubMed](#)]
25. Hamard, J.; Rigal, M.; Gony, M.; Bagheri, H. Lacosamide-induced personality changes: An unexpected adverse effect. *Fundam. Clin. Pharmacol.* **2022**, *36*, 224–226. [[CrossRef](#)]
26. Catterall, W.A.; Goldin, A.L.; Waxman, S.G. International Union of Pharmacology. XLVII. Nomenclature and structure-function relationships of voltage-gated sodium channels. *Pharmacol. Rev.* **2005**, *57*, 397–409. [[CrossRef](#)]
27. Catterall, W.A.; Lenaus, M.J.; Gamal El-Din, T.M. Structure and Pharmacology of Voltage-Gated Sodium and Calcium Channels. *Annu. Rev. Pharmacol. Toxicol.* **2020**, *60*, 133–154. [[CrossRef](#)]
28. Huang, C.-W.; Hung, T.-Y.; Wu, S.-N. The inhibitory actions by lacosamide, a functionalized amino acid, on voltage-gated Na⁺ currents. *Neuroscience* **2015**, *287*, 125–136. [[CrossRef](#)]
29. Wu, S.N.; Lo, Y.C.; Shen, A.Y.; Chen, B.S. Contribution of non-inactivating Na⁺ current induced by oxidizing agents to the firing behavior of neuronal action potentials: Experimental and theoretical studies from NG108-15 neuronal cells. *Chin. J. Physiol.* **2011**, *54*, 19–29. [[CrossRef](#)]
30. Chang, W.T.; Wu, S.N. Characterization of Direct Perturbations on Voltage-Gated Sodium Current by Esaxerenone, a Nonsteroidal Mineralocorticoid Receptor Blocker. *Biomedicines* **2021**, *9*, 549. [[CrossRef](#)]
31. Guérineau, N.C.; Monteil, A.; Lory, P. Sodium background currents in endocrine/neuroendocrine cells: Towards unraveling channel identity and contribution in hormone secretion. *Front. Neuroendocrinol.* **2021**, *63*, 100947. [[CrossRef](#)] [[PubMed](#)]
32. Wu, C.L.; Chuang, C.W.; Cho, H.Y.; Chuang, T.H.; Wu, S.N. The Evidence for Effective Inhibition of I(Na) Produced by Mirogabalin ((1R,5S,6S)-6-(aminomethyl)-3-ethyl-bicyclo[3.2.0]hept-3-ene-6-acetic acid), a Known Blocker of Ca(V) Channels. *Int. J. Mol. Sci.* **2022**, *23*, 3845. [[CrossRef](#)] [[PubMed](#)]
33. Morris, C.E.; Boucher, P.A.; Joós, B. Left-shifted nav channels in injured bilayer: Primary targets for neuroprotective nav antagonists? *Front. Pharmacol.* **2012**, *3*, 19. [[CrossRef](#)] [[PubMed](#)]
34. Taddese, A.; Bean, B.P. Subthreshold sodium current from rapidly inactivating sodium channels drives spontaneous firing of tuberomammillary neurons. *Neuron* **2002**, *33*, 587–600. [[CrossRef](#)]
35. Zhang, X.-Y.; Bi, R.-Y.; Zhang, P.; Gan, Y.-H. Veratridine modifies the gating of human voltage-gated sodium channel Nav1.7. *Acta Pharmacol. Sin.* **2018**, *39*, 1716–1724. [[CrossRef](#)] [[PubMed](#)]
36. Wang, D.W.; Mistry, A.M.; Kahlig, K.M.; Kearney, J.A.; Xiang, J.; George, A.L.J. Propranolol blocks cardiac and neuronal voltage-gated sodium channels. *Front. Pharmacol.* **2010**, *1*, 144. [[CrossRef](#)]
37. Weiser, T.; Qu, Y.; Catterall, W.A.; Scheuer, T. Differential interaction of R-mexiletine with the local anesthetic receptor site on brain and heart sodium channel alpha-subunits. *Mol. Pharmacol.* **1999**, *56*, 1238–1244. [[CrossRef](#)]
38. Simasko, S.M. A background sodium conductance is necessary for spontaneous depolarizations in rat pituitary cell line GH3. *Am. J. Physiol.* **1994**, *266 Pt 1*, C709–C719. [[CrossRef](#)] [[PubMed](#)]
39. Wu, S.-N.; Chen, B.-S.; Hsu, T.-I.; Peng, H.; Wu, Y.-H.; Lo, Y.-C. Analytical studies of rapidly inactivating and noninactivating sodium currents in differentiated NG108-15 neuronal cells. *J. Theor. Biol.* **2009**, *259*, 828–836. [[CrossRef](#)] [[PubMed](#)]
40. Carter, B.C.; Bean, B.P. Incomplete inactivation and rapid recovery of voltage-dependent sodium channels during high-frequency firing in cerebellar Purkinje neurons. *J. Neurophysiol.* **2011**, *105*, 860–871. [[CrossRef](#)]

41. Tsai, D.; Morley, J.W.; Suanning, G.J.; Lovell, N.H. Frequency-dependent reduction of voltage-gated sodium current modulates retinal ganglion cell response rate to electrical stimulation. *J. Neural Eng.* **2011**, *8*, 066007. [[CrossRef](#)] [[PubMed](#)]
42. Ghovanloo, M.-R.; Aimar, K.; Ghadiry-Tavi, R.; Yu, A.; Ruben, P. Physiology and Pathophysiology of Sodium Channel Inactivation. *Curr. Top Membr.* **2016**, *78*, 479–509. [[PubMed](#)]
43. Navarro, M.A.; Salari, A.; Lin, J.L.; Cowan, L.M.; Penington, N.J.; Milesu, M.; Milesu, L.S. Sodium channels implement a molecular leaky integrator that detects action potentials and regulates neuronal firing. *eLife* **2020**, *9*, e54940. [[CrossRef](#)] [[PubMed](#)]
44. Luna, C.; Mizerska, K.; Quirce, S.; Belmonte, C.; Gallar, J.; Acosta, M.D.C.; Meseguer, V. Sodium channel blockers modulate abnormal activity of regenerating nociceptive corneal nerves after surgical lesion. *Investig. Ophthalmol. Vis. Sci.* **2021**, *62*, 2. [[CrossRef](#)]
45. Sula, A.; Hollingworth, D.; Ng, L.C.; Larmore, M.; DeCaen, P.G.; Wallace, B. A tamoxifen receptor within a voltage-gated sodium channel. *Mol. Cell* **2021**, *81*, 1160–1169.e5. [[CrossRef](#)]